

Retrograde predominance of small saturnian moons reiterates a recent retrograde collisional disruption

EDWARD ASHTON,¹ BRETT GLADMAN,² MIKE ALEXANDERSEN,³ AND JEAN-MARC PETIT⁴

¹*Institute of Astronomy and Astrophysics, Academia Sinica, No.1, Sec. 4, Roosevelt Road, Taipei 10617, Taiwan*

²*Dept. of Physics and Astronomy, University of British Columbia, Vancouver BC, Canada*

³*Center for Astrophysics | Harvard & Smithsonian, 60 Garden Street, Cambridge, MA 02138, USA*

⁴*Université Marie et Louis Pasteur, CNRS, Institut UTINAM (UMR 6213), OSU THETA, F-25000 Besançon, France*

(Received March, 2025; Revised December, 2025; Accepted December, 2025)

Submitted to PSJ

ABSTRACT

We report the discovery and careful orbital determination of 64 new irregular moons of Saturn found in images taken using the Canada-France-Hawaii Telescope from 2019-2021, bringing the total number of saturnian irregulars to 122. By more than doubling the sample of saturnian irregular moon orbits, including pushing to smaller sizes, we can now see finer detail in their orbital distribution. We note the emergence of potential subgroups associated with each of Siarnaq and Kiviuq within the Inuit group.

We find that in the inclination range 157–172 degrees the ratio of smaller moons (diameters less than 4 km) to larger moons (diameters greater than 4 km) is significantly larger than that of any other inclination range in the retrogrades. We denote this subset of the Norse group as the Mundilfari subgroup after its largest member. The incredibly steep slope of the Mundilfari subgroup’s size distribution, with a differential power law index of $q = 6$, strengthens the hypothesis in Ashton et al. (2021) that this subgroup was created by a recent catastrophic collision, $< 10^8$ yr ago.

Keywords: irregular satellites — saturnian satellites — Saturn

1. INTRODUCTION

All four giant planets in the Solar System have moons that are thought to be planetesimals that were captured by their host planet during the final stages of planet formation. These moons, known as irregular moons, can be distinguished from their regular counterparts (moons that formed around their host planet as the planet was forming) by their orbits. The semi-major axes of irregular moons are typically much larger than those of regular moons, hundreds of planetary radii versus a few to tens of planetary radii. Additionally, irregular moons have moderate to large orbital eccentricities and a variety of inclinations, whereas the regular moons have near-circular orbits that are situated around the equator of the host planet. See Jewitt & Sheppard (2005), Nicholson et al. (2008), and Denk et al. (2018) for review articles covering saturnian irregular moons.

Phoebe was the first irregular moon of Saturn discovered back in 1898. Since then, excluding the moons found in this work, just two surveys have been able to discover irregular moons around Saturn. A bit more than 100 years after Phoebe’s discovery, Gladman et al. (2001) found 12 irregular moons from images taken in 2000 and 2001 using multiple telescopes with wide-field capabilities. Their orbits yielded the first evidence of inclination groupings for saturnian irregulars.

The other successful survey at finding saturnian irregulars used the Subaru Telescope between 2004 and 2007. Overall, this search was able to discover and track 45 new moons. This survey was eventually outlined in Sheppard et al. (2023). The reviews of Nicholson et al. (2008) and Denk et al. (2018) contain discussions of 25 of the 45 moons from this survey. Combining Phoebe with the moons found in the two aforementioned surveys, a total of 58 saturnian irregulars were known by 2019.

Strong solar perturbations on these distant moons cause periodic oscillations in both inclination and eccentricity, taking ~ 500 yr for saturnians. Thus, time-averaged orbital elements are a more stable measure of an irregular moon’s

orbit than the osculating orbital elements; these time-averaged orbital elements of irregular moons can be calculated using N-body simulations to monitor the evolution of each of the moon's orbital elements over time (see [Nesvorný et al. \(2003\)](#); [Turrini et al. \(2008\)](#); [Jacobson et al. \(2022\)](#)). Simulations need to be integrated over many oscillations to obtain accurate time-averaged elements. Unless otherwise stated, anytime semi-major axis (a), eccentricity (e), or inclination (i) of an irregular moon is mentioned hereafter we refer to the time-averaged value.

Two of the saturnian irregular groups are direct in nature ($i < 90^\circ$, also known as prograde): the Inuit group, with inclinations relative to the ecliptic of $\approx 48^\circ$, and the Gallic group, with inclinations of $\approx 38^\circ$. Both of the direct irregular groups were not well populated, with only six members each pre-2021, and have inclination spreads of only a few degrees. The retrograde ($i > 90^\circ$) Norse group, in contrast, is much more dispersed, with inclinations ranging from 136° to 178° , and contained a vast majority of the saturnian irregulars with 46 members.

The 10° separation between the Gallic and Inuit groups is a factor of two smaller than the up to 20° variation in inclination that a saturnian irregular can experience ([Nesvorný et al. 2003](#); [Turrini et al. 2008](#); [Jacobson et al. 2022](#)), which shows why calculating time-averaged orbital elements is vital for studying the orbital distribution of irregular moons. A good example is Saturn LX, with a current inclination of 44.4° it was initially thought that the moon was a member of the Inuit group. However, when using the time-averaged inclination 38.6° , it was evident that Saturn LX belongs to the Gallic group ([Jacobson et al. 2022](#)).

It was initially thought that a single irregular moon group was created by the break up of a larger moon, like the collisional families seen in the asteroid belt. However, some groups are too dispersed to be explained by a single collision ([Grav et al. 2003](#); [Nesvorný et al. 2003](#); [Turrini et al. 2008](#)). A likely remedy is either multiple independent collisions, second-generation collisions between fragments of the initial collision, or a mixture of the two. Over the years there have been many attempts to divide the groups into subgroups/pairs of saturnian irregulars ([Grav et al. 2003](#); [Grav & Bauer 2007](#); [Turrini et al. 2008](#); [Denk et al. 2018](#); [Ashton et al. 2021](#)). However, these studies had only a small fraction (less than a third) of the currently known saturnian irregulars at their disposal.

Although there is currently no consensus on the exact mechanism by which the initial population of irregular moons was captured, multiple theories have been proposed. The most popular are gas drag by an extended envelop and three-body interactions (either the planet capturing one member of a passing binary, or planetesimal capture during a planet-planet encounter). Refer to [Nicholson et al. \(2008\)](#) for a detailed discussion of the proposed capture scenarios. Knowing the orbital distribution of the initial irregular moon population would provide constraints on the capture mechanism. However, this is complicated by the fact that the irregular moon populations have likely undergone significant collisional alteration over the age of the Solar System ([Bottke et al. 2010](#)). Therefore, understanding the collisional history of an irregular moon system allows one to better constrain the initial population and thus the capture process, realising that only traces of the original captures are currently still present.

This paper details the results of a search for irregular moons of Saturn using the Canada-France-Hawaii Telescope (CFHT) from 2019 to 2021, and an analysis of the saturnian irregular moon population. A summary of the observations and the search method can be found in [section 2](#). The 64 new moons discovered as a result of the survey are described in [section 3](#). Analysis of the orbital distribution is found in [section 4](#). A look at the size distribution of groups/subgroups is presented in [section 5](#). The case for the Mundilfari subgroup being a recent collisional family is detailed in [section 6](#). Finally, we give concluding remarks in [section 7](#).

2. OBSERVATIONS

In the first 4 nights of July, 2019 CFHT acquired images of one of two fields near Saturn (one east and one west of the planet, with offsets shown in [Fig. 1](#)). Each night contained 44 sequential wide-band (gri) images that were acquired over an approximately 3 hour period. The 44 205-sec images from a night were combined using the shift and stack technique ([Gladman et al. 1998](#); [Kavelaars et al. 2004](#); [Ashton et al. 2021](#)) to detect moving irregular moons of Saturn down to diameters, D , of approximately 3 km ($m_w = 26.3$). A total of 120 objects moving at Saturn-like rates were detected, of which 45 were eventually linked to previously designated moons. This search and a debiased size distribution over the entire moon system is detailed in [Ashton et al. \(2021\)](#). At this time, even the orbital sense (i.e. retrograde versus direct) of most of the orbits were not known.

In order to track the remaining 75 candidate moons, to confirm their moon status, and to obtain their orbits, additional observations were acquired. The original plan was to observe both fields in the 3 dark runs following the initial July 2019 observations. However, due to various reasons, images were obtained only in the end of August/ start

of September dark run. Additionally, these nights only went to a depth of $m_w \sim 26$ due to a combination of higher stellar density, extinction due to clouds, and poorer image quality.

Due to inadequate followup observations taken in 2019, more images were acquired in 2020. Both fields were reimaged on two nights each in June, and then one night each a month later in July. The west field got a bonus, but partial, sequence of 29 images in August. A final sequence (for each field) was acquired in July 2021. The same filter, the same field offsets from Saturn, and the same shift and stack technique used for the July 2019 observations were also used in all of the follow-up observations.

3. DETECTIONS

Over all images in our survey we were able to observe all of the 58 previously known saturnian irregulars except for one, Bestla. Bestla's large orbital inclination and node location resulted in it spending a large fraction of its time during these observations nearly due north or south of Saturn, which our fields did not cover (Fig. 1); because other moons of comparable inclinations were both recovered and newly detected, this must partly be a timing issue of where Bestla was at the time. All of the previously known moons now have 14-year observational arcs at the minimum¹, and thus possess very high-precision orbits. Our survey produced 64 new irregular moons of Saturn, details of which are provided below.

3.1. *Finding new moons*

The sparse observations made linking the candidate moons challenging. The method that produced a vast majority of the new discoveries involved linking candidate moons in the 2020 opposition through linear extrapolation to obtain a preliminary orbit from a month arc and then extrapolating this orbit in an attempt to find linkages in the 2019 and 2021 observations. Although linking candidate moons within the 2020 opposition was straightforward, the number of observations in 2020 is so little that most of the orbits were relatively unconstrained. As such, the orbit was able to be significantly altered while still providing a good fit, resulting in many candidate linkages that had to be checked.

The rest of the new moons were confirmed using the same method stated in the previous paragraph but starting with the 2019 observations. However, this method had a couple of setbacks. One being the vast departure of the actual position of the moons from the linear extrapolation over two months, making it challenging to find the July 2019 candidates in the Aug/Sept 2019 observations. The other issue is the relatively shallow depth of the Aug/Sept 2019 images, as detailed in section 2. This meant that only the brightest moon candidates in the July 2019 images were able to be found in the Aug/Sept 2019 data, and thus tracked to the following two oppositions.

In total, 64 new irregular moons of Saturn have been discovered using our data set. One of these, S/2019 S 1 whose very small semi-major axis results in being visible outside Saturn's glare for only a small fraction of the time, was announced in 2021 (Ashton et al. 2022); the rest were announced in May 2023. Additionally, we were able to detect 50+ more moon candidates that we were unable to link together due to an insufficient number of detections.

3.2. *Linking back to past surveys*

Like this survey, the 2003–2007 survey using Subaru (Sheppard et al. 2023) detected many moon candidates that were unable to be connected into a long enough arc to produce confirmed moons. The precision of our multi-year orbits of the new moons is good enough that the Minor Planet Center was able to link back the majority of our linked moons to these previous candidates. Of the 64 new moons, 42 were matched to candidates found by Subaru from 2004–2007, ranging from a single night of observations to seven nights spread over multiple oppositions. If a solar system object is detected on at least two different nights in a single opposition, then the year of the first night becomes the discovery year. As such, 33 of the new moons ultimately have 2004–2007 as their discovery year and have one of those years as part of their temporary designation (see Table 1).

3.3. *July 2019 detections*

Of the 75 moon candidates found in July 2019 that were not linked to a previously known moon, 44 are linked to the new discoveries, leaving 31 candidates from the July 2019 data that are still not yet linked to a confirmed moon. Most of these remaining candidates are faint, with only nine being above the characterisation limit (50% detection efficiency) of the CCD they were found on. An additional 12 more new moons were detected in the July 2019 images.

¹ Even though we did not observe Bestla, another team measured it in 2015, providing a 14-year observational arc.

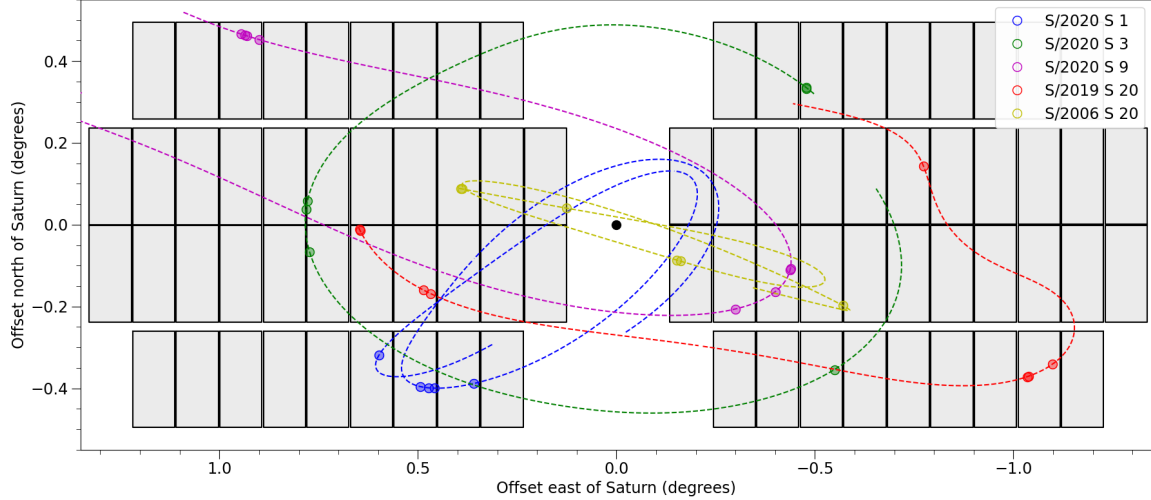


Figure 1. On-sky plot of the two fields used for this survey relative to Saturn (grey rectangles). All measurements of 5 of the 64 new moons detected are shown (circles) along with the best fit orbit (dashed lines). This sub-sample illustrates the challenges of multi-year linking. (Note that the apparent non-closure of the orbits is due to the projected saturnocentric positions being observed from the moving Earth.)

These moons were missed in the original search but were found from high-precision orbits obtained by linking 2020 and 2021 observations.

4. GROUPS

For our analysis of the orbital distribution of the saturnian irregular moons we used the time-averaged orbital elements calculated by JPL². Their methods are detailed in Jacobson et al. (2022), where they simulated the orbits of the 58 irregular saturnian moons known prior to this work, plus S/2019 S 1, over a 5,000 year period. All inclinations are relative to the ecliptic except for Phoebe, which is relative to the Laplace plane.

4.1. Size

Before analysing the saturnian irregular moon population as a whole, we used Equation 5 from Petit et al. (2008),

$$H = m_{\odot} - 2.5 \log \left(\frac{pr^2}{2.25 \times 10^{16}} \right), \quad (1)$$

to estimate each moon's size, where m_{\odot} is the Sun's apparent magnitude, and H , p , and r are the Solar System absolute magnitude, geometric albedo, and radius in km of the moon, respectively. For this equation to be valid, the values for H , p , and m_{\odot} all need to be in the same filter. We will use the V-band filter for our size calculations since that is the filter the Minor Planet Center uses for their values for H of irregular moons³. For $m_{V,\odot}$ we use a value of -26.77, which comes from $M_{V,\odot} = 4.80$ (Willmer 2018). Since only a few of the saturnian irregulars have measured albedos we have decided to go with a single value of $p_V = 0.06$, which is the median value of the three saturnian irregular moons with measured albedos, 0.081 ± 0.02 for Phoebe (Simonelli et al. 1999), 0.06 ± 0.03 for Albiorix, and 0.050 ± 0.017 for Siarnaq (Grav et al. 2015). Substituting in the values for $m_{V,\odot}$ and $p_V = 0.06$, and turning r into D (diameter), Equation 1 becomes

$$\left(\frac{D}{2 \text{ km}} \right)^2 = 10^{0.4(17.2 - H_V)} \quad (2)$$

It should be noted that using a single albedo value means that the slope of the size distribution is independent of the albedo value. Thus, our choice of albedo has little bearing on our analysis.

² <https://ssd.jpl.nasa.gov/sats/elem/#refs>

³ <https://www.minorplanetcenter.net/iau/NatSats/NaturalSatellites.html>

Table 1. A list of the irregular moons of Saturn with their semi-major axis (a), eccentricity (e), inclination (i), orbital period (P), V-band absolute magnitude (H_V), the group they belong to, and the subgroup we have assigned to them (if any). Orbital elements are taken from JPL^c and H_V from MPC^d. All inclinations are relative to the ecliptic except for Phoebe, which is relative to the Laplace plane.

Name/Designation	a (au)	e (10^6 km)	i (deg)	P (days)	H_V	Group	Subgroup
S/2007 S 8	0.1140	17.05	0.49	36.2	836.9	15.97	Gallic
Albiorix (26)	0.1092	16.33	0.48	36.8	783.5	11.17	Gallic
Erriapus (28)	0.1170	17.51	0.476	37.1	871.1	13.71	Gallic
S/2004 S 24	0.1560	23.34	0.071	37.4	1341.3	15.98	Gallic
Tarvos (21)	0.1218	18.22	0.522	37.8	926.4	13.04	Gallic
Bebhionn (37)	0.1138	17.03	0.459	38.5	834.9	14.99	Gallic
Sat LX	0.1140	17.06	0.485	38.6	837.8	15.83	Gallic
S/2006 S 12	0.1308	19.57	0.542	38.6	1035.1	16.2	Gallic
S/2020 S 4	0.1219	18.24	0.495	40.1	926.9	17.01	Gallic
S/2020 S 3	0.1207	18.06	0.142	46.0	908.2	16.38	Inuit
S/2019 S 14	0.1193	17.85	0.172	46.2	893.1	16.32	Inuit
S/2019 S 6	0.1217	18.21	0.120	46.4	919.7	15.73	Inuit
Siarnaq (29)	0.1195	17.88	0.309	47.8	895.6	10.61	Inuit
Kiviuq (24)	0.0756	11.31	0.275	48.0	449.1	12.67	Inuit
S/2005 S 4	0.0757	11.32	0.315	48	450.2	15.69	Inuit
S/2004 S 31	0.1170	17.50	0.159	48.1	866.1	15.63	Inuit
S/2020 S 1	0.0758	11.34	0.337	48.2	451.1	15.92	Inuit
S/2020 S 5	0.1229	18.39	0.22	48.2	933.9	16.59	Inuit
Paaliaq (20)	0.1003	15.00	0.378	48.5	687.0	11.71	Inuit
Tarqeq (52)	0.1186	17.75	0.143	48.7	885.0	14.82	Inuit
Ijiraq (22)	0.0758	11.34	0.293	49.2	451.4	13.27	Inuit
S/2019 S 1	0.0752	11.25	0.384	49.5	445.5	15.32	Inuit
Bestla (39)	0.1360	20.34	0.486	138.3	1087.2	14.61	Norse
Narvi (31)	0.1289	19.29	0.441	142.2	1003.9	14.52	Norse
S/2019 S 11	0.1381	20.66	0.513	144.6	1115.0	16.25	Norse
Hyrrokkin (44)	0.1226	18.34	0.336	149.9	931.9	14.34	Norse
Skathi (27)	0.1041	15.58	0.281	151.6	728.1	14.41	Norse
S/2019 S 19	0.1540	23.04	0.458	151.8	1318.0	16.51	Norse
Kari (45)	0.1473	22.03	0.469	153.0	1231.2	14.49	Norse
S/2004 S 21	0.1548	23.16	0.394	153.2	1328.6	16.21	Norse
S/2004 S 36	0.1564	23.39	0.625	153.3	1349.4	16.11	Norse
S/2004 S 45	0.1316	19.69	0.551	154	1038.7	15.97	Norse
Geirrod (66)	0.1488	22.26	0.539	154.3	1251.1	15.89	Norse
S/2019 S 18	0.1547	23.14	0.509	154.6	1327.1	16.56	Norse
S/2019 S 17	0.1519	22.72	0.546	155.5	1291.4	15.86	Norse
S/2006 S 1	0.1253	18.75	0.105	156.0	964.2	15.65	Norse
S/2006 S 3	0.1427	21.35	0.432	156.1	1174.8	15.65	Norse
S/2019 S 20	0.1583	23.68	0.354	156.1	1375.5	16.73	Norse
Farbauti (40)	0.1356	20.29	0.249	156.2	1087.3	15.75	Norse
S/2019 S 15	0.1416	21.19	0.257	157.8	1161.6	16.59	Norse
S/2004 S 37	0.1066	15.94	0.448	158.2	755.6	15.92	Norse
S/2007 S 5	0.1059	15.84	0.104	158.4	746.9	16.23	Norse
Bergelmir (38)	0.1288	19.27	0.145	158.8	1005.5	15.16	Norse
Thiazzzi (63)	0.1576	23.58	0.512	158.8	1366.7	15.91	Norse
S/2019 S 5	0.1276	19.09	0.216	158.8	990.4	16.65	Norse
Beli (61)	0.1384	20.70	0.087	158.9	1121.7	16.09	Norse
S/2007 S 9	0.1348	20.17	0.360	158.9	1078.1	16.06	Norse
Skoll (47)	0.1178	17.62	0.463	159.4	878.4	15.41	Norse
S/2019 S 9	0.1361	20.36	0.433	159.5	1093.1	16.27	Norse
S/2004 S 49	0.1497	22.40	0.453	159.7	1264.3	15.97	Norse
Gunnlod (62)	0.1413	21.14	0.251	160.3	1158.0	15.57	Norse
S/2004 S 47	0.1073	16.05	0.291	160.9	762.5	16.29	Norse
S/2006 S 15	0.1457	21.80	0.117	161.1	1214.0	16.22	Norse
S/2020 S 7	0.1163	17.40	0.500	161.4	861.2	16.79	Norse
S/2020 S 9	0.1699	25.41	0.531	161.4	1532.6	16.02	Norse
S/2006 S 10	0.1269	18.98	0.151	161.6	983.1	16.43	Norse
S/2020 S 8	0.1469	21.97	0.252	161.8	1228.1	16.41	Norse

^a <https://ssd.jpl.nasa.gov/sats/elem/#refs>

^b <https://www.minorplanetcenter.net/iau/NatSats/NaturalSatellites.html>

^c <https://ssd.jpl.nasa.gov/sats/elements.html>

Table 2. Continuation of Table 1.

Name/	<i>a</i>	<i>e</i>	<i>i</i>	<i>P</i>	<i>H_V</i>	Group	Subgroup
Designation	(au)	(10 ⁶ km)	(deg)	(days)			
S/2004 S 48	0.1480	22.14	0.374	161.9	1242.4	15.95	Norse
S/2006 S 13	0.1334	19.95	0.313	162.0	1060.6	16.05	Norse
S/2019 S 16	0.1556	23.27	0.250	162.0	1340.9	16.68	Norse
S/2004 S 53	0.1556	23.28	0.240	162.6	1342.4	16.16	Norse
Jarnsaxa (50)	0.1288	19.27	0.218	163.0	1006.5	15.62	Norse
Gridr (54)	0.1287	19.25	0.187	163.9	1004.7	15.77	Norse
S/2019 S 10	0.1384	20.70	0.248	163.9	1123.0	16.66	Norse
S/2004 S 50	0.1494	22.35	0.45	164.0	1260.4	16.4	Norse
S/2006 S 16	0.1452	21.72	0.204	164.1	1207.5	16.54	Norse
Fenrir (41)	0.1493	22.33	0.137	164.5	1260.2	15.89	Norse
S/2004 S 12	0.1324	19.80	0.337	164.7	1048.6	15.91	Norse
S/2004 S 7	0.1426	21.33	0.511	164.9	1173.9	15.56	Norse
Eggþther (59)	0.1326	19.84	0.157	165.0	1052.3	15.39	Norse
S/2004 S 52	0.1768	26.45	0.292	165.3	1633.9	16.5	Norse
Hati (43)	0.1317	19.70	0.372	165.4	1040.1	15.45	Norse
S/2020 S 10	0.1692	25.31	0.296	165.6	1527.2	16.86	Norse
S/2004 S 41	0.1210	18.10	0.301	165.7	914.6	16.31	Norse
S/2004 S 42	0.1219	18.24	0.157	165.7	925.9	16.11	Norse
S/2004 S 39	0.1550	23.19	0.101	165.9	1335.9	16.14	Norse
Aegir (36)	0.1381	20.66	0.255	166.1	1119.3	15.51	Norse
S/2007 S 6	0.1239	18.54	0.169	166.5	949.5	16.36	Norse
S/2006 S 14	0.1408	21.06	0.060	166.7	1152.7	16.5	Norse
S/2019 S 3	0.1142	17.08	0.249	166.9	837.7	16.22	Norse
S/2020 S 6	0.1420	21.25	0.480	166.9	1167.9	16.55	Norse
Mundilfari (25)	0.1243	18.59	0.212	166.9	952.9	14.57	Norse
S/2019 S 12	0.1396	20.89	0.475	167.1	1138.9	16.33	Norse
S/2004 S 44	0.1305	19.52	0.129	167.7	1026.2	15.82	Norse
S/2004 S 28	0.1462	21.87	0.159	167.9	1220.7	15.77	Norse
S/2004 S 17	0.1317	19.70	0.162	167.9	1040.9	15.95	Norse
Loge (46)	0.1532	22.92	0.192	166.9	1311.8	15.36	Norse
Sat LXIV	0.1614	24.14	0.280	168.3	1420.8	16.15	Norse
Surtur (48)	0.1521	22.75	0.448	168.4	1295.6	15.77	Norse
S/2006 S 17	0.1496	22.38	0.425	168.7	1264.5	16.01	Norse
S/2004 S 13	0.1233	18.45	0.265	169.0	942.6	16.25	Norse
S/2004 S 40	0.1075	16.08	0.297	169.2	764.6	16.28	Norse
S/2007 S 7	0.1065	15.93	0.217	169.2	754.3	16.24	Norse
S/2005 S 5	0.1428	21.37	0.588	169.5	1177.8	16.36	Norse
S/2006 S 18	0.1521	22.76	0.131	169.5	1298.4	16.1	Norse
Fornjot (42)	0.1667	24.94	0.213	170.0	1494.1	15.12	Norse
S/2019 S 4	0.1200	17.95	0.408	170.1	903.9	16.46	Norse
S/2020 S 2	0.1195	17.87	0.152	170.7	897.6	16.89	Norse
S/2004 S 43	0.1266	18.94	0.432	171.1	980.1	16.34	Norse
S/2004 S 51	0.1685	25.21	0.201	171.2	1519.4	16.13	Norse
S/2019 S 21	0.1767	26.44	0.155	171.9	1636.4	16.18	Norse
Ymir (19)	0.1534	22.95	0.338	172.3	1315.1	12.41	Norse
S/2019 S 8	0.1356	20.29	0.311	172.8	1088.9	16.28	Norse
Sat LVIII	0.1745	26.10	0.147	173.0	1604.0	15.7	Norse
S/2006 S 9	0.0963	14.41	0.248	173.0	647.9	16.48	Norse
S/2006 S 20	0.0882	13.19	0.206	173.1	567.3	15.75	Norse
S/2019 S 2	0.1107	16.56	0.279	173.3	799.8	16.49	Norse
S/2007 S 3	0.1311	19.61	0.150	173.8	1034.4	15.74	Norse
S/2007 S 2	0.1066	15.94	0.232	174.0	754.9	15.59	Norse
S/2006 S 11	0.1318	19.71	0.143	174.1	1042.3	16.47	Norse
Greip (51)	0.1229	18.38	0.317	174.1	937.0	15.33	Norse
S/2019 S 7	0.1349	20.18	0.232	174.2	1080.6	16.29	Norse
Gerd (57)	0.1400	20.95	0.518	174.4	1143.0	15.87	Norse
Thrymr (30)	0.1359	20.33	0.467	175.0	1092.2	14.33	Norse
Phoebe (9)	0.0864	12.93	0.164	175.2	550.3	6.73	Norse
S/2006 S 19	0.1591	23.80	0.467	175.5	1389.3	16.07	Norse
Skrymir (56)	0.1434	21.45	0.437	175.6	1185.1	15.62	Norse
Suttungr (23)	0.1296	19.39	0.116	175.7	1016.7	14.55	Norse
S/2004 S 46	0.1371	20.51	0.249	177.2	1107.6	16.4	Norse
S/2019 S 13	0.1401	20.96	0.318	177.3	1144.8	16.68	Norse
Alvaldi (65)	0.1470	21.99	0.238	177.4	1232.2	15.62	Norse
Angrboda (55)	0.1376	20.59	0.216	177.7	1114.1	16.17	Norse

4.2. *Gallic Group*

The Gallic group only gained three new members, which makes it now 9 moons in total (see Figure 2). Of the six previously known Gallic group members, all but S/2004 S 24 have similar a . This clustering, which we will refer to as the Albiorix subgroup, also includes all three of the new members. Interestingly, Albiorix has the lowest a of all known Gallic members. Perhaps the Albiorix subgroup, or even the Gallic group as a whole, was created via a cratering event on the leading hemisphere of Albiorix, with this still (mostly) intact parent body remaining close to its pre-collision orbit. If the crater location was near the apex point of Albiorix's velocity, all the fragments would be ejected in the direction of the leading hemisphere; their relative Δv boost would have some component in the direction of motion of the parent body, producing larger a (see subsection 6.1). Such a leading-hemisphere impact event is greatly favoured when the projectile is moving in the opposite orbital sense from the target, and naturally results in a higher relative impact speed (about twice the orbital speed for a direct encounter), allowing retrograde projectiles to provide a much larger kinetic energy to the impact. Given that there are significantly more retrograde irregular moons compared to direct ones, a leading-hemisphere collision is a plausible scenario.

One of the new Gallic moons, S/2006 S 12, has reduced the size of the semi-major axis gap between the Albiorix subgroup and S/2004 S 24 but this gap still remains larger than the pericentre of S/2004 S 24. The disconnect of S/2004 S 24 from the rest of the group, in terms of having a significantly larger a and being the only Gallic member whose perihelion is not lower than the semi-major axis of Albiorix itself, means that the question still remains whether S/2004 S 24 comes from the same parent body as the rest of the Gallic group. We explore this further in subsection 6.1.

4.3. *Inuit Group*

The Inuit group has more than doubled their number of known members, from 6 to 13. With the addition of these new Inuit moons, some structure within the group has become clear (see Figure 2). All of the new Inuit moons have semi-major axes close to that of a previously known moon, producing two subgroups which were both mentioned by Sheppard et al. (2023).

Three of the new Inuit moons, S/2019 S 1, S/2020 S 1, and S/2005 S 4, have very similar a to Kiviuq and Ijiraq, creating a subgroup within the Inuit group. The pair of Kiviuq and Ijiraq has long been thought to have a common origin (Turrini et al. 2008; Denk et al. 2018). Thus, with the addition of the new moons, it has become clear that the Kiviuq subgroup (named after the largest member) is highly likely a collisional family with very low velocity dispersion.

There is a similar case with the moons surrounding Siarnaq. When there was only Tarqeq with similar a and i to Siarnaq, Denk et al. (2018) labelled the two as a potential co-orbiting pair that separated. Since then S/2004 S 31 and now the new moons of S/2019 S 6, S/2020 S 3, S/2020 S 5, and S/2019 S 14 have been revealed to have orbits similar to that of Siarnaq. Thus, the Siarnaq subgroup, consisting of 7 members, is likely another collisional family in the Inuit group.

Interestingly, unlike the rest of the Inuit members, Paaliaq currently does not have any companions that share similar a . Perhaps Paaliaq, with an a that is about halfway between the Kiviuq and Siarnaq subgroups, is part of a cluster, but the other members are too small to be detected currently.

The big question about the Inuit group still remains: Do all members share a common origin? One scenario is that the Inuit group originated from a single moon that has been broken up by multiple collisions. Although it is hard to imagine how three distinct clusterings with a large variation in semi-major axes can arise from what was initially a single object. Another scenario is that the Kiviuq subgroup, the Siarnaq subgroup, and Paaliaq are not related to each other. However, the probability that three unrelated clusterings share a similar i is very low, especially since there appears to be only one other direct group in the saturnian system. Perhaps they initially had different inclinations and over time they became aligned, although such a mechanism is currently unknown.

4.4. *Norse Group*

Gladman et al. (2001) initially suggested that Skathi (S/2000 S 8) should be kept separate from the rest of the so-called Phoebe subgroup due to its significantly different orbital inclination; in the end, all retrograde saturnians have been receiving norse-themed names. Even the postulated 'Phoebe group' was remarked to be unusual, in that Phoebe is very much larger than the other 4 discoveries from 2000: Ymir, Thrymr, Suttungr (which have Phoebe-like inclinations but much larger semi-major axes) and Mundilfari, which has an inclination offset from Phoebe much larger than the spread seen in the two direct inclination groups).

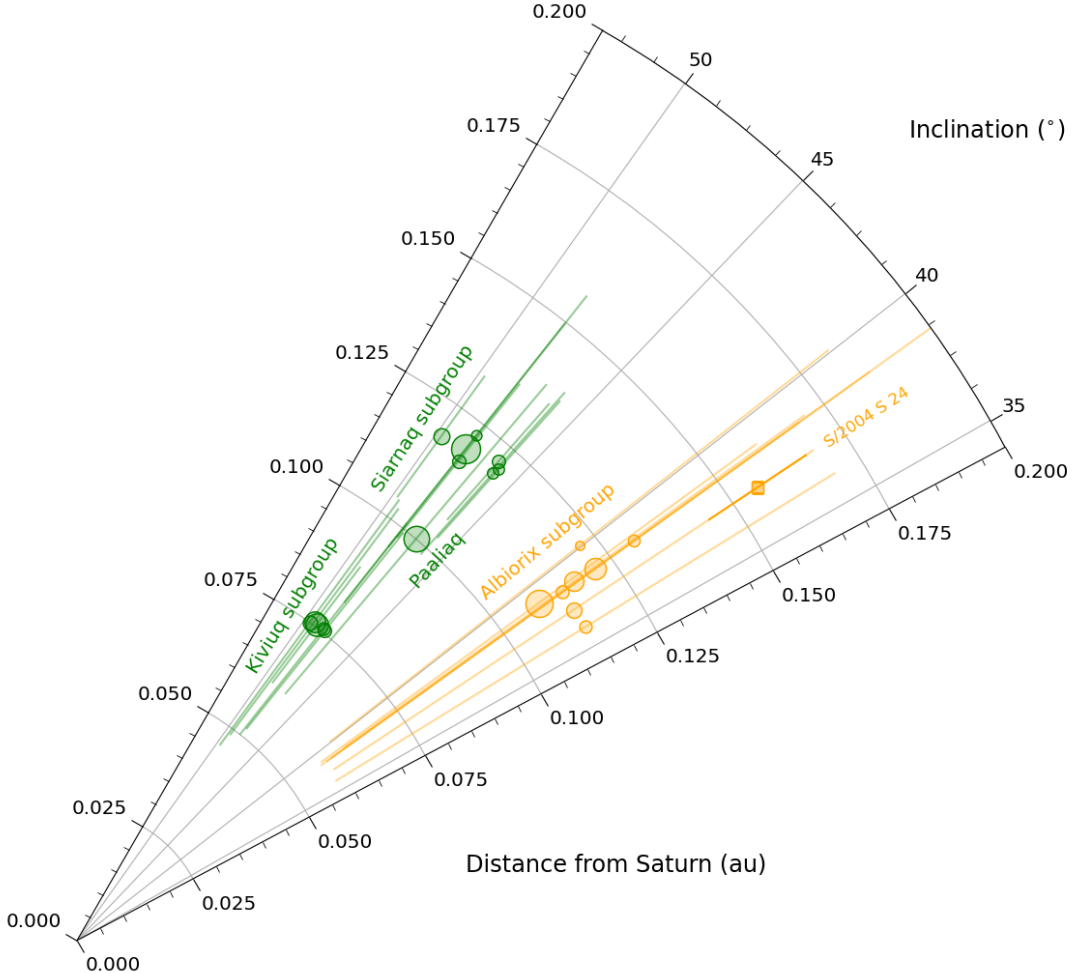


Figure 2. Rose diagram of the irregular moons of Saturn with direct orbits. Each circle represents the time averaged inclination and semi-major axis of a moon, with the size of the circle indicating the relative size of the moon. Additionally, each moon has a line that goes from the time-averaged pericentre to the time-averaged apocentre. Yellow represents moons that belong to the Gallic group, and green represents the Inuit group. The gap between S/2004 S 24 (represented by a square instead of a circle) and the rest of the Gallic group has decreased with the inclusion of the new moons, but still remains large (see subsection 4.2 for discussion).

Like the previously known moons, the vast majority of the new moons belong to the Norse/retrograde group. Of the 64 new moons, 54 are Norse group members. This is a slightly larger fraction than that of previously known moons (46/58). The retrograde population has now exploded in number into a very complicated distribution that is far more difficult to interpret than the tightly-clustered direct groups. At first glance, the rose plot of the retrograde moons (Figure 3) does not cleanly manifest much structure in the orbital distribution. Looking at a cumulative inclination distribution, however, it appears that the Norse group can be broken up by using inclination cuts tied to subtle features (top panel of Figure 4).

4.4.1. Phoebe Subgroup

Ashton et al. (2021) attempted to subdivide the Norse group by defining the Phoebe subgroup as moons with inclinations within 3° of Phoebe's value. From the top panel of Figure 4 a clear absence of moons (relative to surrounding inclinations) can be seen at 172° , suggesting there is a division between Phoebe-like inclinations and the rest. This division can be seen more clearly when looking at just the large ($D > 4$ km) Norse members (bottom panel of Figure 4). Here we will use the criteria $i > 172^\circ$ to define the Phoebe subgroup (although, currently, we get the

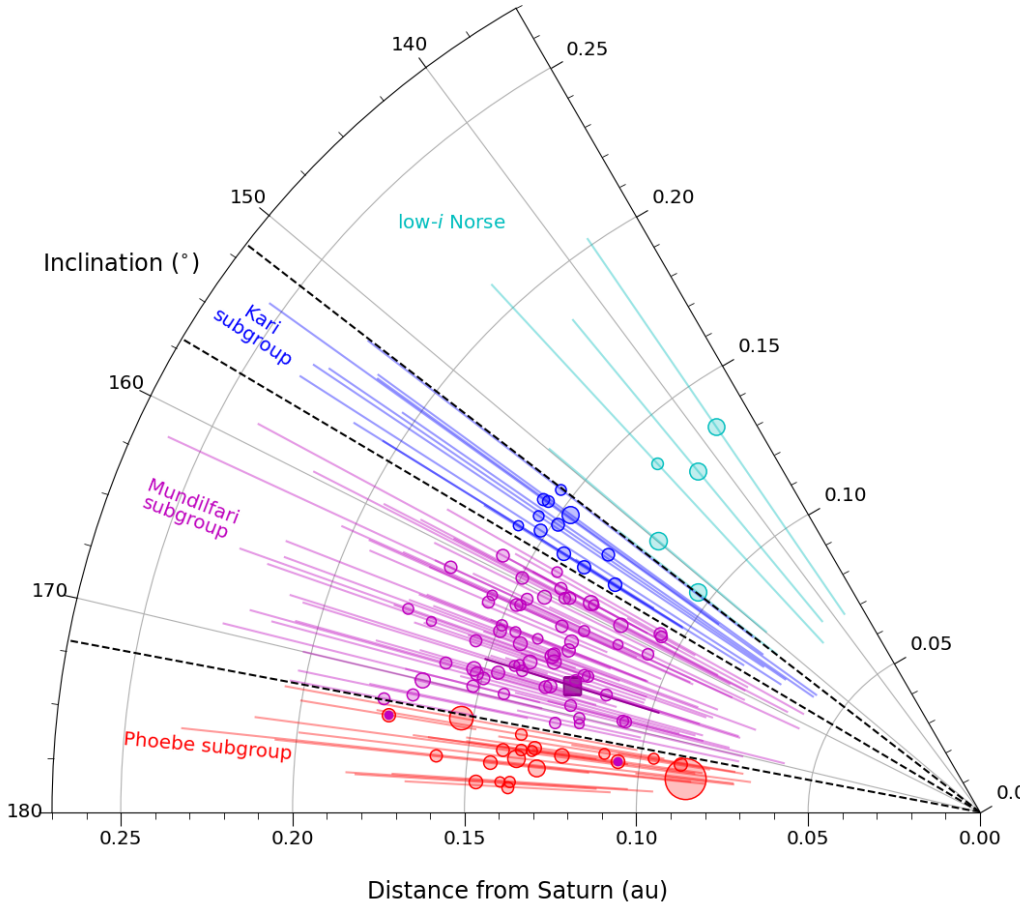


Figure 3. Rose diagram of the retrograde saturnian irregulars. See Fig. 2’s caption. Here, red represents moons belonging to the Phoebe subgroup, magenta represents the Mundilfari subgroup, blue represents the Kari subgroup, and cyan represents low- i ($<151^\circ$) Norse members. Mundilfari is represented by a square and is a darker shade of purple, in order to distinguish the moon from the rest of the subgroup named after it. Two Phoebe subgroup members that may be outlying members of the Mundilfari subgroup are indicated with an additional inset magenta dot.

same Phoebe subgroup members if we use the criteria from Ashton et al. (2021)). The recent batch of new discoveries has added 10 more members to the Phoebe subgroup for a total of 21 (see Table 1 for the full list).

We caution, however, that the saturnocentric distance variation of a large fraction of the Phoebe subgroup members do not overlap with that of Phoebe (i.e. the pericenter of some members is larger than the apocenter of Phoebe). As such, a scenario of the subgroup being created by a single collision off Phoebe seems unlikely. There is a small clustering in Phoebe subgroup members around 20×10^6 km $\simeq 0.13$ au which may be a good candidate for a small collisional subfamily. Furthermore, there are four moons, Angrboda, Alvaldi, S/2019 S 13, and S/2004 S 46, which have similar $a \sim 0.14$ au and i , 177.2 – 177.7° . This close clustering in i , and the fact that they are 1.6° away from the rest of the Phoebe subgroup (see Figure 4), could be an indication of another small collisional subfamily. Curiously, the large irregular Ymir is still quite isolated at $a \simeq 0.15$ au and $i \simeq 172^\circ$. Lastly, the lowest- a members of the Phoebe subgroup, S/2006 S 9 and S/2006 S 20 (maybe even S/2019 S 2 and S/2007 S 2 too), could be fragments of a cratering event off Phoebe.

4.4.2. Kari Subgroup and low inclination Norse moons

At the low- i end of the Norse group (closest to $i = 90^\circ$) the cumulative distribution (top panel of Figure 4) flattens out when going to smaller i . This flattening occurs at two i ’s, 157° and 152.5° . This suggests that these i ’s might be good locations for having subgroup boundaries. We decided to extend the lower limit to 151.7° so that this subgroup

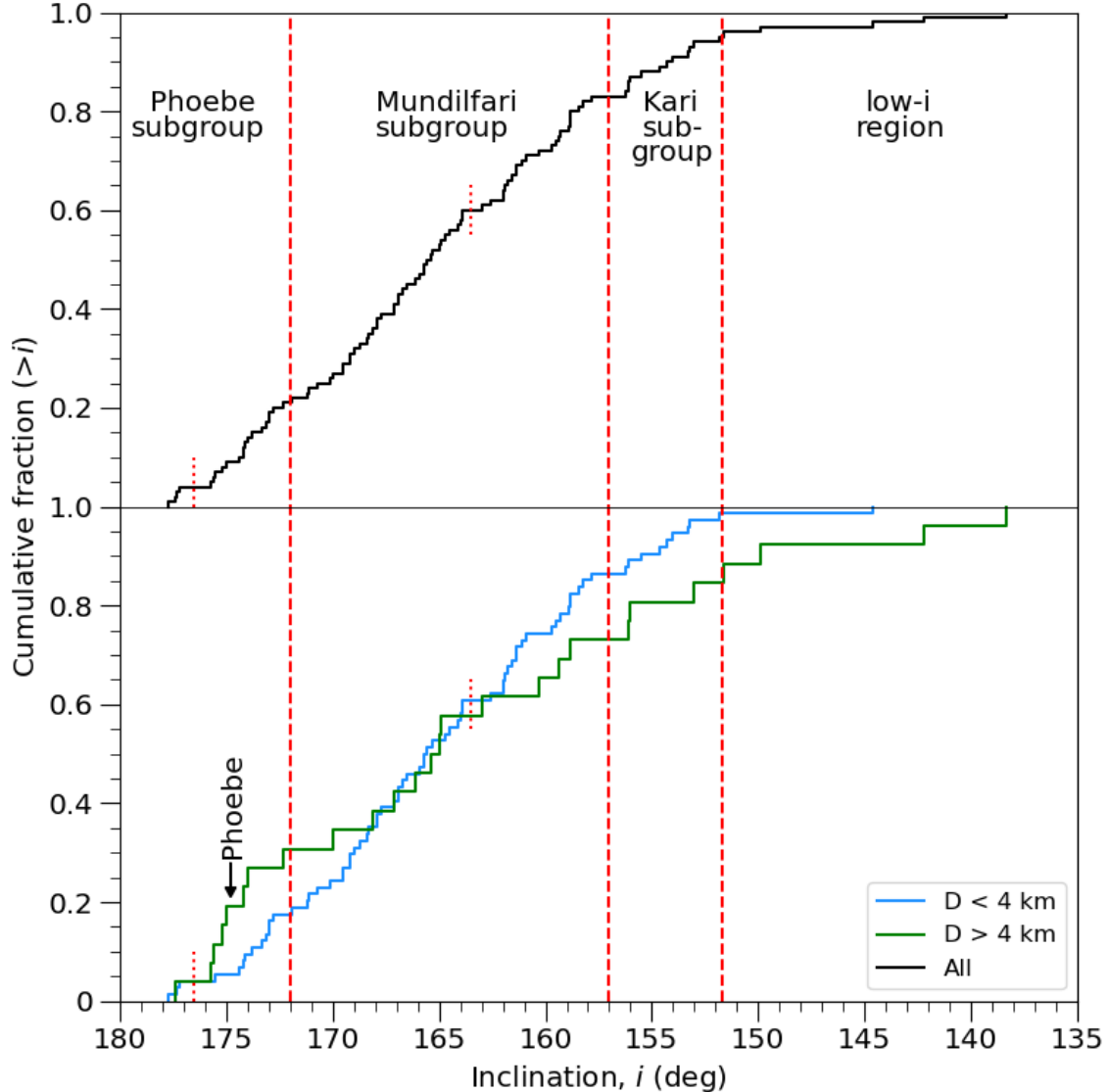


Figure 4. Inverse cumulative inclination distribution of the full Norse/retrograde population (top panel) and then split up into large (> 4 km) and small (< 4 km) members (bottom panel). We divide the Norse group up into three sub-groups with red dashed lines marking the boundaries. There are two sets of short red dotted lines in each panel, one at 176.5° indicating a potential further subdivision within the Phoebe subgroup (see subsubsection 4.4.1) and one at 163° indicating a minor dearth of moons within the Mundilfari subgroup (see subsection 5.1).

includes S/2019 S 19, which has a a similar to that of a majority of the subgroup members. As such, we define the Kari subgroup (named after the largest member) as the moons with $151.7^\circ < i < 157^\circ$. The tightly packed nature of the Kari subgroup, without the 3-4 lowest a members, makes it a good candidate for a collisional family.

Of the five Norse moons with the lowest i , which were the only moons not placed in any subgroups, Skathi and Hyrrokkin could potentially be related (although there is a large separation between their a 's). Narvi, S/2019 S 11, and Bestla have similar a 's but are a bit spread in i . We note that this population is approaching $i = 90^\circ$ closely enough that the Kozai effect may begin to operate, like that observed for three Inuit moons by Jacobson et al. (2022), with the potential for long-term instability of the moons Gladman et al. (2001) setting a boundary for this group.

4.4.3. Mundilfari Subgroup

The remaining Norse moons (with $157^\circ > i > 172^\circ$) are put into what we denote the Mundilfari subgroup. This subgroup could actually be broken into two as there is a dearth of moons around i of 163° (top panel of Figure 4).

However, both regions of the Mundilfari subgroup that are divided by the $i = 163^\circ$ line have significantly higher fractions of small ($D < 4$ km) Norse moons compared with the fractions of large ($D > 4$ km) Norse moons (bottom panel of Figure 4). All the other inclination ranges either have fractions of large moons that are similar or larger than that of small moons (currently). This suggests that both of these two i ranges have significantly steeper size distributions compared to the other saturnian irregulars. As such, we have kept it as one subgroup. Further discussion of size distributions is presented in section 5.

Using the inclination distribution is a good method to define Norse subgroups as collisional fragments will clump together in i . Although, having just a single i as the boundary between groups will most likely result in moons being put into sub-groups that they do not belong to. Two good examples of this are discussed in section 5.

5. SIZE DISTRIBUTION

Although the inclination study was done first, and the boundaries of these divisions are obviously not very strong, we later discovered that the splits as we made them resulted in a dramatically different size distribution for the Mundilfari subgroup when compared to all other saturnians. When one splits up the saturnian irregular size distribution into different groups/subgroups (Figure 5) one can see that the Mundilfari subgroup is significantly steeper than the other clusters over a large range of diameters. As shown by one of the reference slopes (dotted line) in Figure 5 the Mundilfari subgroup has a fairly consistent differential power law index, q , of approximately 6 down until at least $D \sim 3$ km, at which point incompleteness causes the distribution to flatten out.

The other two Norse subgroups, Phoebe and Kari, generally have much less steep slopes in the same size range (3–6 km), similar to that of collisional equilibrium, $q = 3.5$ (Dohnanyi 1969). Even shallower still are the two direct groups, Gallic and Inuit, which both have shallow slopes of $q \sim 2$ throughout.

Both the Phoebe and Kari subgroups have a narrow size range around 4 km where the size distributions have similar steepness to that of the Mundilfari subgroup. As mentioned in subsubsection 4.4.3, there is likely cross-contamination between what we have defined as subgroups. In the size range where the Phoebe subgroup has a very steep slope (3.7–4.7 km), 4 out of the 8 members have i within 2° of the Mundilfari subgroup (i.e. $172^\circ < i < 174^\circ$). One of the four moons is S/2006 S 20 which, as mentioned in subsubsection 4.4.1 is likely a collisional fragment off of Phoebe. Another is S/2007 S 3, with an a of 0.1311 au, is at the outer edge of a large cluster within the Phoebe subgroup, and is thus more likely to be associated with this cluster and not to the Mundilfari subgroup. The other two moons, S/2007 S 2 and Sat LVIII, could easily belong to the Mundilfari subgroup, as they are fairly isolated in a - i (see Figure 3). Additionally, Sat LVIII has a similar a to Mundilfari members just on the other side of the inclination divide. If both of these moons are indeed members of the Mundilfari subgroup and not the Phoebe subgroup, the slope of the size distribution at around 4 km would be significantly shallower for the Phoebe subgroup. A similar argument could be made for the Kari subgroup. After Kari, the next three largest members, S/2006 S 3, S/2006 S 1, and Farbauti, are all within 1° of the Mundilfari boundary and all have a 's lower than the main Kari subgroup cluster. Additionally, small-number statistics might play a part.

Ashton et al. (2021) found that the saturnian irregulars, as a whole, had $q = 4.9$ from $D = 3$ to 4 km and postulated that this steep slope was due to a recent collision (in the last Gyr). Catastrophic collisions (and cratering events) are known to produce steep size distributions (see Durda et al. (2007) for example). They were unable to determine which members were likely involved in the collision as almost all of the moons that they detected in the size range did not have known orbits at the time. However, they did suggest that it was likely located in the retrograde population. The new saturnian irregulars discovered show that the Mundilfari subgroup alone is essentially the cause of the steep size distribution found by Ashton et al. (2021). Thus, we believe that it is the Mundilfari subgroup that was created by the recent collision hypothesised by Ashton et al. (2021). If this is true then the Mundilfari collisional family is significantly more dispersed in a and i than the other potential collisional families seen among the irregular moons.

5.1. Splitting up the Mundilfari Subgroup

We explore the idea that perhaps this steep slope is only present in a subset of the Mundilfari subgroup. If the subgroup is split into two by a potential division at $i = 163^\circ$, as discussed in subsubsection 4.4.3, the slope of the size distributions of the two regions are very similar to that of the Mundilfari subgroup as a whole (see left panel in Figure 6). Additionally, we split the Mundilfari subgroup into two subsamples two different ways using cuts of $a = 0.14$ au or $e = 0.25$. The values of the a and e cuts were chosen to split the Mundilfari subgroup into roughly equal numbers. Like with the i split, the size distribution of the high/low e/a all have very high slopes, like the Mundilfari

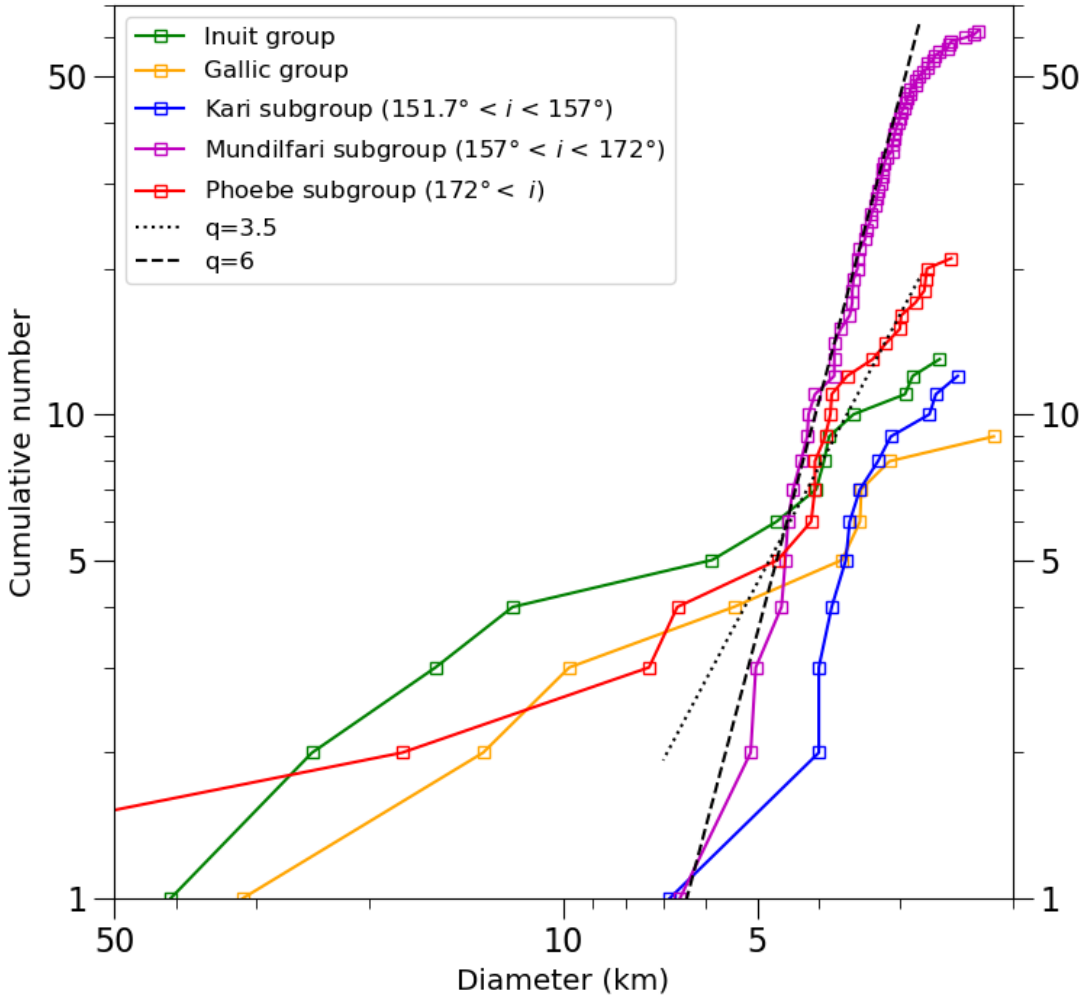


Figure 5. Size distribution of different groups/subgroups in the saturnian irregular moon population. The method used to calculate diameters is described in subsection 4.1. Two lines have been added for reference, one with a collisional equilibrium, $q = 3.5$ (dotted line), and one with a similar slope to that of the Mundilfari subgroup, $q = 6$ (dashed line). Note: the five $i < 151^\circ$ Norse group members are not represented in this plot.

subgroup as a whole (middle and right panels in Figure 6, respectively); the $e < 0.25$ sample has the shallowest slope with $q \sim 5$. We therefore believe that the steep slope present in all subdivisions justifies our choice to keep the Mundilfari subgroup intact.

5.2. Observational Bias

A caveat that must be taken into consideration is that the sample has not been debiased. Even though a majority of saturnian irregulars lie in the two offset fields (Fig. 1) at any one instant, and the two fields have been observed many times over multiple oppositions, this survey is still somewhat biased towards moons with certain orbits. The lack of coverage north and south of Saturn (see Figure 1) results in moons with i closer to 90° being harder to detect compared to moons with i closer to 0 or 180° . This is exemplified by the fact that we never imaged Bestla, the lowest i Norse group member. Another bias, identified in Ashton et al. (2022), is that the glare from Saturn makes it harder to detect moons with smaller a or pericentre. Given these two biases, the Inuit and Gallic subgroups and the low- i Norse

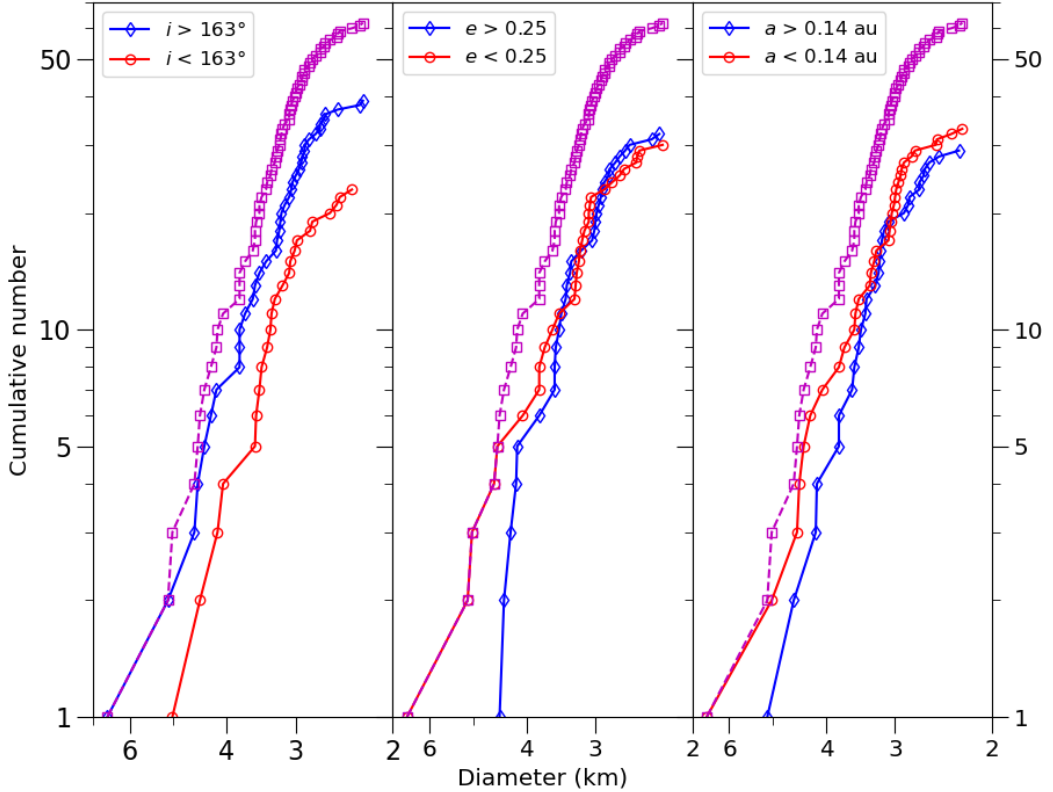


Figure 6. A comparison of the size distributions of the Mundilfari subgroup when split into two samples using cuts in inclination (left panel), eccentricity (middle panel), and semi-major axis (right panel). The size distribution of the whole Mundilfari subgroup is shown in magenta in all panels.

moons ($i < 151^\circ$) are likely under-represented in the current sample, and thus have size distributions that are likely more steep in reality than what is seen in Figure 5. The Norse subgroups, on the other hand, are less affected by such observational biases, with the possible exceptions of the low- a part of the Phoebe subgroup and, to a lesser extent, the Kari subgroup. Therefore, we believe that observational biases in our survey should not influence our analysis or conclusions regarding the Mundilfari subgroup.

6. COLLISIONAL FAMILIES SIMULATIONS

Some of the clusters of saturnian irregular moons are tight enough that they could easily be created by a single disruption event (e.g. the Kiviuq subgroup and the Siarnaq subgroup). On the other hand, the Gallic group and the Mundilfari subgroup have comparatively larger orbital spread, and, as such, we want to test the feasibility of a single collision creating either of these two clusters.

We calculate the orbital extent of a debris field by generating n ejecta particles by adding a fixed $\Delta\mathbf{v}$ in random directions to that of the progenitor velocity at the moment of collision, similar to what was done in Grav et al. (2003). To be judged as to realistically reproducing a clustering, we use the criteria that at least one of the generated ejecta must overlap with the secular ranges of a , e , and i (found in Jacobson et al. (2022)) of every moon in that cluster. There are aspects which make this current analysis somewhat approximate. Firstly, we did not look at the 3 dimensional $a - e - i$ space, just the $a - e$ and $a - i$ space. Secondly, when Jacobson et al. (2022) did their analysis, only one of the 64 new moons was announced, so do not have the computed orbital variations. Thus, we cannot know whether the ejecta correctly recreate the full range of either cluster.

6.1. Gallic group

As mentioned in subsection 4.2, the Gallic group could be created by a head-on cratering event near the apex point of Albiorix. Thus, for the orbit of the progenitor moon, we used the averaged a , e , and i of Albiorix, 0.1092 au, 0.48, and 36.8° respectively. To crudely simulate a head-on cratering collision we restricted the ejecta to having outbound trajectories that are within 90° of the direction of motion of the progenitor. To recreate the comparatively high- a low- e orbit of S/2004 S 24, we set the collision to occur while the progenitor was at apocenter (with true anomaly $f = 180^\circ$). The longitude of ascending node, Ω , argument of periapsis, ω , were set to 0° and 90° , respectively, to match the small inclination range of the group and the fact that the inclinations of almost all members are greater than that of Albiorix. In order to get ejecta out to the distance of S/2004 S 24 one needs a Δv of 330 m/s (see Figure 7). This velocity is significantly higher than what is expected for an irregular moon collisional family (see Turrini et al. (2008) and subsubsection 6.2.1). Additionally, although the ejecta overlap with the e ranges of all Gallic group members (that have ranges), there appears to be a trend (sans S/2004 S 24) that the larger a members also have slightly larger e .

We next turn our attention to just the Albiorix subgroup (this is the Gallic group without S/2004 S 24). To get an ejecta cloud that has increasing e with increasing a , we changed ω to 120° and f to 30° . To reach the outermost member of the Albiorix subgroup, S/2006 S 12, a Δv of 80 m/s is needed (see Figure 7). This much lower Δv , compared with the Gallic group as a whole, is well within the acceptable range for a collisional family (see Turrini et al. (2008) and subsubsection 6.2.1). Thus, the Albiorix subgroup itself is a good candidates for a collisional family.

As for the origin of S/2004 S 24, perhaps there was a secondary collision where one of the larger a Albiorix subgroup members was impacted while near apocenter and S/2004 S 24 is the largest fragment of that collision. Alternatively, as suggested by Sheppard et al. (2023), S/2004 S 24 might not be related to the rest of the Gallic group and, coincidentally, happen to have similar i . Discovering more Gallic group members should lead to a better understanding of the origin of S/2004 S 24.

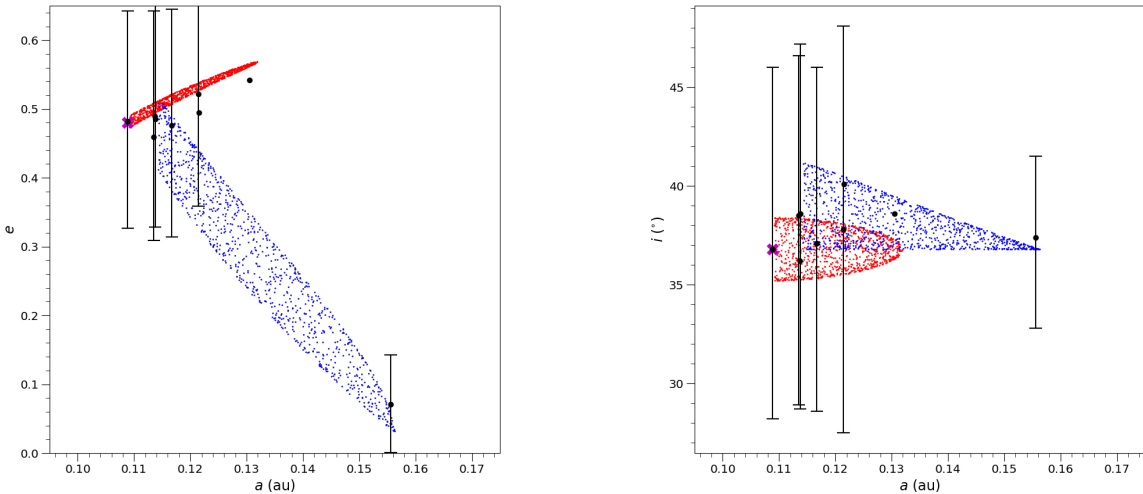


Figure 7. A thousand ejecta particles were simulated in attempt to recreate the spread in orbit of the Gallic group with S/2004 S 24 and without. The ejecta particles were created by adding $\Delta v = 80$ m/s (red dots) or 330 m/s (blue dots) to that of the chosen progenitor (magenta cross). Time-averaged orbital elements from JPL of all of the moons in the subgroup are shown by black circles. The vertical bars through some of the real moons indicate the range of orbital values that a moon oscillates over during a secular cycle, taken from Jacobson et al. (2022). The variations in a are typically comparatively small and are thus not shown. The orbital elements ranges of the newest moons are not shown since they were announced after the Jacobson et al. (2022) study and are therefore not provided by JPL.

6.2. Mundilfari subgroup

As mentioned in section 5 there is evidence that the entire Mundilfari subgroup was created by a recent catastrophic collision. To test this, we used the approximate centre of the Mundilfari subgroup for i , a , and e as the orbit of the progenitor, with values of 165° , 0.126 au, and 0.28 respectively. We varied Ω , ω , and f to find an ejecta field that best matched the orbits of the Mundilfari subgroup. Since this subgroup is more dispersed in orbital element space, we have increased the number of simulated ejecta to 2000.

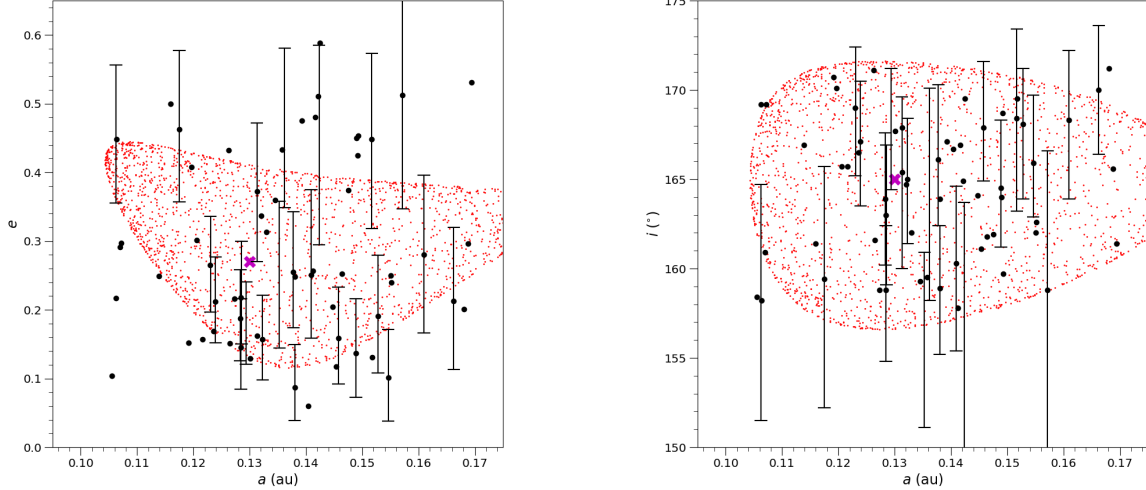


Figure 8. An attempt to recreate the spread in orbit of the Mundilfari subgroup members (black) by simulating 2000 ejecta particles (red). The ejecta particles were created by adding $\Delta v = 200$ m/s in a random direction to that of a chosen progenitor (magenta cross). See Figure 7 caption for more details.

We find that a minimum of 200 m/s is needed for Δv to produce an ejecta field that covers the ranges of almost all of the Mundilfari subgroup members (see Figure 8). This occurred when the progenitor had $\Omega \simeq 0^\circ$, $\omega \simeq 270^\circ$, and $f \simeq 240^\circ$. It was much easier to fit the spread in i compared to the spread in e and a .

6.2.1. Velocity Dispersion

Based on hydrocode models, Nesvorný et al. (2003) set a velocity dispersion limit of 100 m/s to identify potential collisional families within the saturnian irregular moon population, where the velocity dispersion for a set of moons is obtained using Gauss equations. In Turrini et al. (2008), they decided to relax the limit to 200 m/s to account for the large oscillations that the orbits of irregular moons can have. Although our minimum Δv is the same as the velocity dispersion limit used by Turrini et al. (2008), the two velocities are not quite equivalent. Velocity dispersions are calculated using the mean orbital elements, whereas we fit the range of orbital elements.

The Cluster C family defined in Table 3 of Turrini et al. (2008) contains 11 of 13 Mundilfari subgroup members known then, and additionally Griep, Farbauti, and S/2006 S 1 (all of which have inclinations close to the limits that define the Mundilfari subgroup, see section 5). Due to the similarities in the members of the Mundilfari subgroup and the Cluster C family, the velocity dispersions of the two sets of moons should be very similar. Since Turrini et al. (2008) found that the Cluster C family has a velocity dispersion of 240 m/s, the velocity dispersion for the Mundilfari subgroup likely exceeds 200 m/s. If one accepts this criterion, the Mundilfari subgroup appears to be too dispersed to be a collisional family.

Perhaps some members at the extrema a and/or e of the Mundilfari subgroup were not formed from the recent collision (thus causing the spread in a and/or e of the collisional family to appear larger than it actually is) or perhaps the orbital spread has been enlarged by subsequent collisions within the subgroup but not enough to grind down the steep size distribution. Alternately, it could be that there were two (or more) separate collisions that both occurred recently and overlapped slightly in orbital phase space. Li & Christou (2018) found that the gravitational interaction with Phoebe causes ejecta from the large moon to disperse over the age of the Solar System. However, the effect of Phoebe on the spread of the Mundilfari subgroup is likely minimal due to the likely recency of the subgroup and, to

a lesser extent, the lower rate of Phoebe interactions due to the larger mutual inclinations (than what Phoebe impact ejecta would have).

The Himalia group around Jupiter is another cluster of irregular moons that is a good candidate for a collisional family but again with a velocity dispersion that appears too high (Nesvorný et al. 2003). With more than one candidate collisional family in the irregular moon population having more dispersion in orbital phase space than is expected, perhaps some detail in the understanding of irregular moon collisions is missing.

6.2.2. Colours

Numerous works have measured the colours of saturnian irregulars (Grav et al. 2003; Buratti et al. 2005; Grav & Bauer 2007; Graykowski & Jewitt 2018; Peña & Fuentes 2022), although with the main focus of comparing saturnian irregulars, along with irregular moons of other giant planets, to other populations of small bodies in the Solar System. There has been very little attempt to use colour information to identify potential collisional families. This is mainly due to the difficulty of getting high-quality colours of a large enough sample of saturnian irregulars, caused by the faintness of almost all of the moons coupled with their irregular shapes.

Interestingly, Grav & Bauer (2007) found that Mundilfari has a V-I colour of 0.52 ± 0.07 , significantly bluer than almost any other saturnian irregular. The only saturnian irregular that has similar V-I is Phoebe with 0.64 ± 0.01 . Thus far, V-I colours (or the equivalent g-i in the Sloan filter system) have not been measured for any other Mundilfari subgroup member. Aegir and Fornjot were included in the sample from Graykowski & Jewitt (2018), but they did not obtain observations in the I filter. Peña & Fuentes (2022) observed Skoll, Fornjot, and Loge but did not provide *g*-band magnitudes for these three moons. If the Mundilfari subgroup is indeed a collisional family, then we expect that other members will also exhibit blue V-I colours that Mundilfari is observed to have.

7. CONCLUSION

Irregular moons have likely undergone significant collisional evolution since being captured early in the Solar Systems history. This evolution can be inferred from the current orbital distribution of an irregular moon population. From the discovery and precise tracking of 64 new irregular moons of Saturn, increasing the known number twice fold, we are able to accurately divide the known groups into subgroups. In the Inuit group, we identify two tightly packed subgroups, the Kiviuq and Siarnaq subgroups, each of which are likely to be collisional families. Using the inclination distribution, we split the Norse group into 3 subgroups, which we refer to as the Phoebe, Mundilfari, and Kari subgroups.

The Mundilfari subgroup, with differential size index $q=6$, has a significantly steeper size distribution slope compared to all other groups/subgroups. Due to the steep size distribution, we believe that the Mundilfari subgroup was created by the recent collision proposed by Ashton et al. (2021). A major concern, however, is the large orbital phase space that the Mundilfari subgroup occupies, which is larger than one might expect for the spread coming from the break-up speed of a collisional family. The recent collision hypothesis would be greatly strengthened if other members of the Mundilfari subgroup were found to have the very blue V-I colour of Mundilfari.

8. ACKNOWLEDGMENTS

This work was supported by funding from the Natural Sciences and Engineering Research Council of Canada. Thanks to the CFHT Queue Observing team, especially Todd Burdullis and Daniel Devost, for helping us with the data acquisition process. This research used the facilities of the Canadian Astronomy Data Centre operated by the National Research Council of Canada with the support of the Canadian Space Agency.

REFERENCES

Ashton, E., Gladman, B., & Beaudoin, M. 2021, *PSJ*, 2, 158

Ashton, E., Gladman, B., Beaudoin, M., Alexandersen, M., & Petit, J.-M. 2022, *PSJ*, 3, 107

Bottke, W. F., Nesvorný, D., Vokrouhlický, D., & Morbidelli, A. 2010, *AJ*, 139, 994

Buratti, B. J., Hicks, M. D., & Davies, A. 2005, *Icarus*, 175, 490

Denk, T., Mottola, S., Tosi, F., Bottke, W. F., & Hamilton, D. P. 2018, in *Enceladus and the Icy Moons of Saturn*, ed. P. M. Schenk, R. N. Clark, C. J. A. Howett, A. J. Verbiscer, & J. H. Waite, 409

Dohnanyi, J. S. 1969, *J. Geophys. Res.*, 74, 2531

Durda, D. D., Bottke, W. F., Nesvorný, D., et al. 2007, *Icarus*, 186, 498

Gladman, B., Kavelaars, J. J., Nicholson, P. D., Loredo, T. J., & Burns, J. A. 1998, *AJ*, 116, 2042

Gladman, B., Kavelaars, J. J., Holman, M., et al. 2001, *Nature*, 412, 163

Grav, T., & Bauer, J. 2007, *Icarus*, 191, 267

Grav, T., Bauer, J. M., Mainzer, A. K., et al. 2015, *ApJ*, 809, 3

Grav, T., Holman, M. J., Gladman, B. J., & Aksnes, K. 2003, *Icarus*, 166, 33

Graykowski, A., & Jewitt, D. 2018, *AJ*, 155, 184

Jacobson, R. A., Brozović, M., Mastrodemos, N., Riedel, J. E., & Sheppard, S. S. 2022, *AJ*, 164, 240

Jewitt, D., & Sheppard, S. 2005, *SSRv*, 116, 441

Kavelaars, J. J., Holman, M. J., Grav, T., et al. 2004, *Icarus*, 169, 474

Li, D., & Christou, A. A. 2018, *Icarus*, 310, 77

Nesvorný, D., Alvarellos, J. L. A., Dones, L., & Levison, H. F. 2003, *AJ*, 126, 398

Nicholson, P. D., Cuk, M., Sheppard, S. S., Nesvorný, D., & Johnson, T. V. 2008, in *The Solar System Beyond Neptune*, ed. M. A. Barucci, H. Boehnhardt, D. P. Cruikshank, A. Morbidelli, & R. Dotson, 411–424

Peña, J., & Fuentes, C. 2022, *AJ*, 163, 274

Petit, J. M., Kavelaars, J. J., Gladman, B., & Loredo, T. 2008, in *The Solar System Beyond Neptune*, ed. M. A. Barucci, H. Boehnhardt, D. P. Cruikshank, A. Morbidelli, & R. Dotson, 71–87

Sheppard, S. S., Tholen, D. J., Alexandersen, M., & Trujillo, C. A. 2023, *Research Notes of the AAS*, 7, 100. <https://dx.doi.org/10.3847/2515-5172/acd766>

Simonelli, D. P., Kay, J., Adinolfi, D., et al. 1999, *Icarus*, 138, 249

Turrimi, D., Marzari, F., & Beust, H. 2008, *MNRAS*, 391, 1029

Willmer, C. N. A. 2018, *ApJS*, 236, 47